BIBECHANA
Vol. 22, No. 3, December 2025, 205-214

ISSN 2091-0762 (Print), 2382-5340 (Online)
Journal homepage: http://nepjol.info/index.php/BIBECHANA
Publisher:Dept. of Phys., Mahendra Morang A. M. Campus (Tribhuvan University)Biratnagar

Hydrogen bonding, spectroscopic (FT-IR and FT-Raman), UV-Vis, and Mulliken charge analysis of Guanosine-5 -Diphosphate: insight from DFT and molecular docking

Manoj Kumar Chaudhary[1], Tarun Chaudhary[2], Bhawani Datt Joshi[3] Gulab Singh Verma[4], Rajesh Kumar Shukla[4], Tirth Raj Paneru[5,6,*]

[1]*Department of Physics, Tribhuvan University, Amrit Campus, Institute of Science and Technology, Kathmandu 44600,Nepal*
[2]*Department of Physics, Bageshwari Multiple Campus, Mid-West University, Kohalpur, 21900, Nepal*
[3]*Department of Physics, Tribhuvan University, Siddhanath Science Campus, Mahendranagar, 10400, Nepal*
[4]*Department of Physics, University of Lucknow, Lucknow-226007, India*
[5]*Central Department of General Science, Far Western University, Mahendranagar, 10400, Nepal*
[6]*Central Department of Physics, Tribhuvan University, Kathmandu, Nepal*
[*]Corresponding author. Email: tirthpaneru2015@gmail.com

Abstract

Hybrid functional B3LYP has been used for quantum chemical calculation of Guanosine-5 -Diphosphate (GDP) from DFT approach. The intra-molecular hydrogen bonding in the title molecule was rendered from Quantum theory of atoms in molecule (QTAIM). The vibrations of different functional groups of the GDP have been examined theoretically from FT-IR and FT-Raman calculation. The electrostatic potential (ESP) surface revealed that the maximum positive potential is attributed to H4, and the highest negative potential corresponds to O31, predicting the sites for the intermolecular hydrogen bonding in the crystal packing of the title compound. The theoretical UV-Vis spectrum is used to calculate the excitation energy as well as excitation state of DGP. The binding affinity of GDP with Ras-related C3 botulinum toxin substrate 1 (RAC1) protein is calculated from molecular docking approach. The inhibition constant of 2P2L is less than that of 2H7V; hence, the title compound is a good inhibitor of 2P2L.

Keywords

Guanosine-5 -Diphosphate (GDP); AIM; FT-IR; FT-Raman; molecular docking.

Article information

Manuscript received: January 25, 2025; Revised June 1, 2025; Accepted: July 26, 2025
DOI https://doi.org/10.3126/bibechana.v22i3.74596

1 Introduction

Guanosine is a purine nucleoside with neuroprotective properties, particularly in ischemic stroke, spinal cord injury, and depression. It also reduces neuro-inflammation and oxidative stress [1]. The nucleotides guanosine 5-monophosphate (GMP), guanosine 5-diphosphate (GDP), and guanosine 5-triphosphate (GTP) are the basis of guanine-based purines (GBPs). Ecto-nucleotidases can convert these nucleotides into guanosine [2]. GDP is nucleotides made up of guanine, ribose and two phosphate groups [3]. It has wide applications in biological activity like: cellular signaling and metabolism. GDP is formed due to hydrolysis of guanosine triphosphate (GTP) and there is the evolution of energy which is used in cellular processes. Moreover, GDP take part in the conversion of succinyl-CoA to succinate and there is the production of energy [4]. When GDP is changed into GTP due to activation of G-proteins then signals are transmitted into the cell. GDP has crucial role to maintain the cell structure as well as it is involved in intracellular transport properties by the formation and deformation of microtubules [5, 6].

The functional groups present in GDP are amine group (-NH2), amide group (-C=O-N), hydroxyl group (-OH) and phosphate group (PO_4^{2-}). These functional groups have crucial role to take part in hydrogen bonding in crystal structure as well as in ligand-protein interaction. This study aims to provide insight into reactive parts of GDP by highlighting the sites of intra- and intermolecular hydrogen bonding. The atomic charge on each atom of the title molecule revealed from Mulliken charge analysis. The vibrational spectroscopic techniques (FT-IR and FT-Raman), along with UV-Vis spectroscopy, conducted through quantum chemical calculations, elucidated the vibrations and electronic transitions of significant functional groups in the compound, confirming their role in biological activity. Moreover, the binding affinity of the title compound with the targeted protein was evaluated through molecular docking to assess its biological performance.

2 Materials and Methods

Quantum chemical calculation has been conducted from Gaussian 16 software [7]. The exchange - correlation functional B3LYP was used in this calculation [8–10]. The diffused as well as polarization functional basis set 6-311++G(d,p) is taken into consideration to obtain the more accurate result [11]. The density functional theory (DFT) [12]is the wonder full technique which gives the result closer to experimental value and this is implemented in Gaussian 16 software. The GaussView 06 software [13] is used to visualize the data which is obtained after calculation. The intra-molecular hydrogen bonding in the investigated molecule has been calculated from quantum theory of atoms in molecule (QTAIM) by using AIMALL software package [14, 15]. The RDG isosurface, scatterplot, and molecular electrostatic potential mapped into the molecular surface produced by the Multiwfn 8.0 and VMD 1.9.1 software packages [16, 17]. The ligand-protein interaction of GDP with predicted target RAC1 is explored from AutoDock and Discovery Studio Visualizer 4.5 [18, 19]. The Gauss Sum software has been implemented to explore the excitation state and excitation energy from UV-Vis spectroscopy [20].

3 Results and Discussion

3.1 Atoms in molecules (AIM)

he intra-molecular hydrogen bonding of GDP has been explored by using QTAIM analysis [15]. The judgement of intra-molecular hydrogen bonding in GDP is based on the electron density (ρ_{BCP}), Laplacian of electron density ($\nabla^2\rho_{BCP}$), and total electron density (H_{BCP}) at bond critical point (BCP). If the respective value of (ρ_{BCP}) and ($\nabla^2\rho_{BCP}$) lies in the range (0.0020.034) a.u and (0.0240.139) a.u, then there is the existence of hydrogen bonding [21]. The nature and strength of hydrogen bonding is identified in terms of ($\nabla^2\rho_{BCP}$) and H_{BCP}. If their values are greater than zero, then there should be weak hydrogen bond (electrostatic). If $(\nabla^2\rho_{BCP}) > 0$ and $H_{BCP} < 0$; then there should be partially covalent bond. If $((\nabla^2\rho_{BCP}))$ < 0 and $H_{BCP} < 0$; there should be strong covalent hydrogen bond [22]. The optimized structure of the GDP with atom numbering scheme is depicted in Figure 1. The molecular graph of GDP highlighting intra-molecular hydrogen bonds is presented in Figure 2. The Table 1 represents the bond length (Å), bond angle (°) and sum of van der Waal radii of interacting atoms ($r_H + r_A$). The value of (ρ_{BCP}), $\nabla^2(\rho_{BCP})$, electron kinetic energy density (G_{BCP}), electron potential energy density (V_{BCP}), total electron energy density (H_{BCP}), and interaction energy (E_{int}) at BCP for GDP is presented in Table 2. The distance between interacting atoms is less than the value of $r_H + r_A$ but $(\nabla^2\rho_{BCP}) > 0$ and $H_{BCP} < 0$ so all the four intra-molecular hydrogen bonds are partially covalent in nature. Moreover, the interaction energy (E_{int}) at BCP for O10-H11...O2 is highest (8.311) kcal/mol, and the bond length H11…O2 is least (1.813 Å) so, H11…O2 is the strongest intra-molecular hydrogen bond out of four.

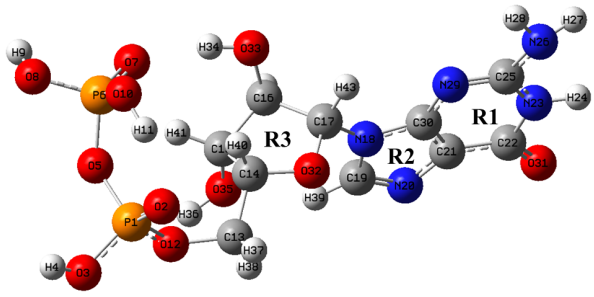

Figure 1: 3D structure of GDP obtained from B3LYP/6-311++G(d,p) level of theory

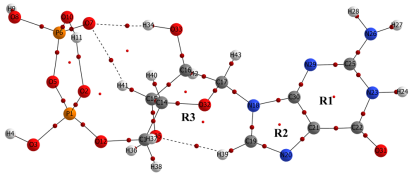

Figure 2: Molecular graph of GDP for intramolecular hydrogen bond.

Table 1: Geometrical parameters for intramolecular hydrogen bonds in GDP: bond length (Å), bond angle (°), and sum of van der Waals radii of interacting atoms ($r_H + r_A$) in Å.

D–H···A	D–H (Å)	H···A (Å)	D–H···A (°)	$r_H + r_A$ (Å)
C19–H39···O35	1.078	2.316	134.291	2.72
C15–H41···O7	1.090	2.405	135.688	2.72
O33–H34···O7	0.970	2.016	161.390	2.72
O10–H11···O2	0.987	1.813	148.943	2.72

Table 2: Topological parameters for intramolecular interaction of GDP: electron density at the bond critical point (ρ_{BCP}), Laplacian of ($\nabla^2\rho_{\mathrm{BCP}}$), electron kinetic energy density (G_{BCP}), electron potential energy density (V_{BCP}), total electron energy density (H_{BCP}), and interaction energy (E_{int}) at the BCP.

Interaction	Bond Length (Å)	ρ_{BCP} (a.u.)	$\nabla^2\rho_{\mathrm{BCP}}$ (a.u.)	G_{BCP} (a.u.)	V_{BCP} (a.u.)	H_{BCP} (a.u.)	E_{int} (kcal/mol)
H39···O35	2.315	0.0114	0.0427	-0.0019	-0.0069	-0.0088	-2.155
H41···O7	2.405	0.0103	0.0353	-0.0014	-0.0062	-0.0076	-1.937
H34···O7	2.014	0.0170	0.0710	-0.0029	-0.0119	-0.0148	-3.748
H11···O2	1.813	0.0310	0.1093	-0.0005	-0.0265	-0.0270	-8.311

3.2 Non-covalent interaction analysis

The non-covalent interaction analysis employed a reduced density gradient (RDG) scatterplot to visualize various interactions in the chemical system using electron density and its derivative. The graph between the sign(λ_2)ρ and a dimensionless parameter RDG insight into the intensity of the interaction. The value of RDG can be evaluated by the following equation: [23, 24]

$$RDG(r) = \frac{1}{2(3\pi^2)^{\frac{1}{3}}} \frac{|\nabla\rho(r)|}{\rho(r)^{\frac{4}{3}}}$$

Different colour codes are used for different types of non-covalent interactions. Weak van der Waals force of attraction is represented by green with the value of sign(λ_2)ρ ≈0. Steric repulsion between interacting species is represented by red with the value of sign(λ_2)$\rho > 0$ and strong hydrogen bonding interaction is represented by blue, with the value of sign(λ_2)$\rho < 0$ [25]. The 2D-NCI RDG graph and its 3D isosurface for the visualisation of non-covalent interaction are shown in Figs, 3 (a) and (b). The RDG isosurface illustrates that the green colour flaky patches appeared between oxygen and hydrogen and nitrogen and hydrogen, which represent the van der Waals interactions between them that are seen in the RDG scatter graph in the region of 0.01 to 0.005 a.u. The red spikes seen in the RDG scatter graph cover a wide range from 0.01 to 0.05 a.u., highlighting the repulsion between the carbon atoms of rings R1, R2, and R3, which is dominant over hydrogen bonding and van der Waals force of attraction. The strong intramolecular hydrogen bond between H11 and O2 is seen in the isosurface by the blue colour, which is observed in the RDG scatter graph with blue spikes in the range of 0.03 to 0.05 a.u. NCI analysis reveals that the intra-molecular hydrogen bonds H39...O35, H41...O7, and H34...O7 exhibit weak van der Waals forces of attraction, while the intra-molecular hydrogen bond O10-H11...O2 is a strong hydrogen bond, which was also justified by QTAIM analysis.

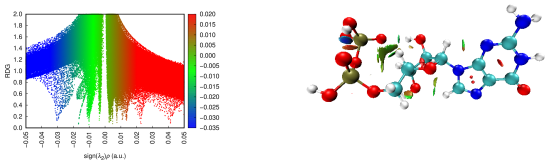

(a) (b)

Figure 3: (a) RDG scatter plot of GDP and (b) 3D isosurface showing non-covalent interactions in GDP.

3.3 Spectroscopic studies

he number of mode of vibration of the molecular system is explained by the relation 3N-6, where N is the number of atoms in the molecule. The GDP molecule has 43 atoms so there are 123 modes of vibration. The FT-IR and the FT-Raman of the investigated molecule has been examined from same level of theory. The calculated spectrum of FT-IR is presented in Figure 4 and the calculated FT-Raman is presented in Figure 5. The DFT calculation is used to obtain the Raman intensities but it depends on the Raman scattering amplitudes and the Raman scattering cross-section $\frac{\partial \sigma_j}{\partial \Omega}$. The Raman scattering amplitude gives Raman intensity for each normal mode of vibration and is given by the relation [26, 27].

$$\frac{\partial \sigma_j}{\partial \Omega} = \left(\frac{2^4\pi^4}{45}\right)\left(\frac{(\nu_0 - \nu_j)^4}{1 - exp\left[\frac{-hc\nu_j}{kT}\right]}\right)\left(\frac{h}{8\pi^2 c\nu_j}\right) S_j$$

where Sj= scattering activities, ν_j = predicted wave numbers for jth normal mode, ν_0= wavenumber of Raman excited state and h, c and k are universal constants.

The calculated wavenumber is more than the experimental one due to anharmonicity. So, to reduce the calculated wave number the linear wavenumber linear scaling (WLS) factor is used [28, 29]. The functional groups are the active parts of GDP and can play a vital role in biological action through different intermolecular interactions. These active parts also participate in intra-molecular hydrogen bonding. The signature of functional groups are seen in higher wavenumber in pure form but the signature at lower wave number is determined the fingerprint regions of GDP and they are in mixed mode. In this study, we only discussed the modes of vibrations related to the signature of functional groups that are seen in higher wavenumbers and are important in biological action. The vibration modes of active parts belong to a functional group and are assigned to higher wavenumber regions along with unscaled and scaled wavenumbers, which are presented in Table 3. The vibrational modes associated with the active groups of GDP are discussed in detail in the following sections.

3.3.1 C=O and P=O vibrations

The experimental value of N–H stretching vibrations is found in the order of (3500-3300) cm^{-1} [30]. In the GDP compound, asymmetric N26H$_2$ stretching is calculated at 3493 cm^1, but its symmetric stretching is calculated at 3396 cm^1. The stretching of N23H vibration is computed at 3412 cm^1 with a significant peak in the FT-IR spectra. The in-plane bending of the amine group N26H$_2$ is calculated at 1630 cm^{-1}and 1585 cm^{-1}with significant IR absorbance. In the title compound, the signatures of CN vibration in rings R1 and R2 are examined at 1556, 1528, and 1487 cm^{-1}with sharp peaks. Experimental OH stretching is generally found in the range (35003200) cm^{-1} [31]. In the title compound, the OH stretching is calculated from DFT at 3633, 3621, 3619, 3517, and 3236 cm^1, corresponding to O35H, O8H, O3H, O33H, and O10H, respectively. The amine group and hydroxyl group has significant peaks in IR and Raman spectroscopy and these functional groups interact with residue of amino acid which is justified in the molecular docking section.

Table 3: The scaled and unscaled wavenumber along with the mode of vibration of different functional groups in GDP.

Unscaled Wavenumber (cm^{-1})	Scaled Wavenumber (cm^{-1})	Types of Vibration
3841	3631	ν(OH) stretching vibration of O35H
3827	3621	ν(OH) stretching vibration of O8H
3824	3619	ν(OH) stretching vibration of O3H
3709	3517	ν(OH) stretching vibration of O33H
3681	3493	$\nu_a(NH_2)$ asymmetric stretching of $N26H_2$
3591	3412	ν(NH) stretching vibration of N23H
3574	3397	$\nu_s(NH_2)$ symmetric stretching of $N26H_2$
3394	3236	ν(OH) stretching vibration of O10H
3263	3118	$R_2[\nu(CH)]$ stretching vibration of C19H
3165	3029	$\nu_a(CH_2)$ asymmetric stretching of $C13H_2$
3110	2979	$R_3[\nu(CH)]$ stretching vibration of C17H
3104	2974	$R_3[\nu(CH)]$ stretching vibration of C15H
3098	2969	$\nu_s(CH_2)$ symmetric stretching of $C13H_2$
3059	2933	$R_3[\nu(CH)]$ stretching vibration of C16H
2994	2874	$R_3[\nu(CH)]$ stretching vibration of C14H
1787	1750	$R_3[\nu(C{=}O)]$ stretching vibration of C22=O
1661	1630	$\delta_{in}(NH_2)$ in-plane bending of $N26H_2$
1614	1585	$\delta_{in}(NH_2)$ in-plane bending of $N26H_2$
1583	1556	ν(CN) vibration of CN in Ring (R_1 and R_2)
1554	1528	ν(CN) vibration of CN in Ring (R_1 and R_2)
1511	1487	ν(CN) vibration of CN in Ring (R_1 and R_2)
1505	1481	$\delta_{in}(CH_2)$ in-plane bending of $C13H_2$
1452	1431	$R_3[\delta_{in}(CH)]$ in-plane bending of C17H
1439	1418	$R_2[\delta_{ring}]$ ring deformation of R_2
1437	1416	$\gamma(CH_2)$ twisting of $C15H_2$
1415	1395	$R_3[\delta_{in}(CH)]$ in-plane bending of CH
1407	1387	δ_{in}(OH) in-plane bending of O33H
1384	1365	$\omega(CH_2)$ wagging of $C13H_2$
1291	1275	ν(P=O) stretching vibration of P6O7
1247	1233	ν(P=O) stretching vibration of P1O2
1166	1154	δ_{in}(OH) in-plane bending of O10H
953	946	δ_{in}(OH) in-plane bending of O8H and P6O10 stretching
871	866	δ_{in}(P6-O10-O8) in-plane bending
865	860	$R_2[\delta_{in}(CH)]$ in-plane bending of C19H
863	859	$R_2[\delta_{in}(CH)]$ in-plane bending of C19H

3.3.2 CH vibration

The experimental C-H stretching vibration is obtained in the range (3000-3100) cm^{-1} [31]. In the title compound, the stretching of C19H, C17H, C15H, C16H, and C14H in the rings R2 and R3 are calculated at 3118, 2979, 2974, 2933, and 2874 cm^1, respectively being very sharp peak for C14H with higher IR absorbance. The in-plane bending of CH vibration is computed at 1431 and 1395 cm^{-1} in the ring R2. For ring R3, the in-plane bending of CH found to be at 860 and 859 cm^{-1}. The asymmetric stretching vibration of $C13H_2$ is calculated at 3029 cm^{-1} but symmetric stretching of $C13H_2$ is calculated at 2969 cm^{-1}.

3.4 Electrostatic potential surface (ESP) analysis

The visual representation of the charge distribution on the molecular surface can be performed by the electrostatic potential surface analysis. This tool aids in the prediction of sites for the intra- and intermolecular interactions by identifying the locations of electrophiles and nucleophiles [32]. The region of positive potential shown by the blue colour region corresponds to the position of the electrophile, which should be favourable for nucleophilic attack, and the negative potential region represented by the red colour is the site of electrophilic attack [33]. The molecular surface of the title compound mapped with the electrostatic potential on its van der Waals surface is shown in Figure 6. The blue and orange dots of the molecular electrostatic surface represent the points of minimum and maximum potential. The global minimum potential of -95.53 kcal/mol attributed to the O31 atom in the C=O group of ring R1 of GDP is the nucleophile. The maximum positive potential 113.71 kcal/mol corresponds to the H4 atom attached to the OH group in phosphate, making it the best site for nucleophilic attack. From this result, we conclude that H4 and O31 are ideal sites for intermolecular hydrogen bonding, and the crystal packing of the title compound may be contributed

by the O3-H4. . . O31 hydrogen bonding.

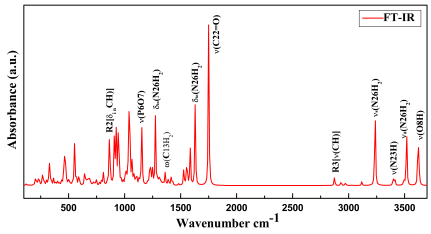

Figure 4: Calculated FT-IR spectra of Guanosine-5 - Diphosphate in the range (100-3800) cm^{-1} calculated from B3LYP/6-311++G(d,p) level of theory.

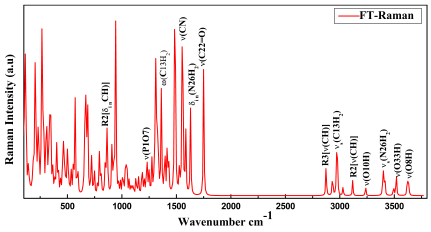

Figure 5: Calculated FT-Raman spectra of Guanosine-5 - Diphosphate in the range (100-3800) cm^{-1} calculated from B3LYP/6-311++G(d,p) level of theory.

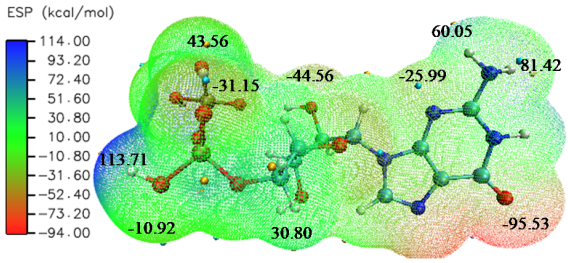

Figure 6: Electrostatic potential mapped into molecular vdW surface of Guanosine-5 - Diphosphate.

3.5 Mulliken Charge Analysis

The electronic property of atom in molecular system has been identified from Mulliken charge analysis. This is calculated on the basis of distribution of electrons in the atoms as well as the formation of polarity in the molecular system [34]. This analysis helps to identify the electrophilic and nucleophilic atoms in the compound that can take part in chemical reaction with surrounding species in hydrogen bonding in crystal packing and ligand-protein interaction [35].

The distribution of charge on the heavy atoms of GDP is presented in Figure 7. From this analysis it is clear that the concentration of negative charge is mainly on O2, O5, O7, C17, N29, C30, and O31. Out of these atoms, the highest value of negative charge is seen on C17. This is due to shearing of charge among C16, N18 and O32 atoms. Similarly, the concentration of positive charge is more across P6, N18 and C19. But the highest value of positive charge is calculated across N18. These atoms have prominent role to take part in ligand-protein reaction.

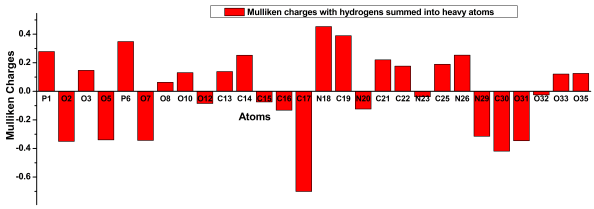

Figure 7: Mulliken charge with hydrogen summed into heavy atoms on GDP from B3LYP/6-311++G(d,p).

3.6 UV-Visible Spectra Analysis

The essential and useful technique to study the biologically active compounds is UV-Vis spectroscopy. The spectrum helps in the characterization of substances and gives an idea regarding their electronic structure. The spectrum is used to check biological activity of compounds when changes are made to functional groups that insure the change in (increase or decrease) drug activity of molecules when derivatives are synthesized [35]. Besides these activities, it also helps with compound stability, activity quantification, and interaction monitoring which are critical for assessing and maximizing biological activity. UV-Vis spectroscopy can monitor enzyme activity in real time; it helps to study the photo stability of biologically active compounds [36]. It helps to quantify the changes in absorbance upon binding, indicating interaction mechanisms, binding constants, and binding sites. Moreover, it helps to examine the electronic structure, aromatic rings, and functional group present in the compound and the band gap energy of compound to check the nature of compound whether it is semiconductor or other type of materials [37, 38]. Besides that it has wide applications to measure the concentration and interaction of proteins and nucleic acids as well as it is used to study the enzyme activity. The UV-Vis spectra of GDP is calculated in gaseous state by employing the TD-B3LYP/6-311++G(d,p) the-

ory. The UV-Vis spectra is plotted which is presented in Figure 8. The absorption peak is obtained at 271 nm which infer that there is delocalization of -electron due to guanine base which contains conjugated double bonds and aromatic ring in GDP. In guanine base structure there is also absorption of lone pair electrons η due to presence of nitrogen (N) and Oxygen (O) atoms in GDP. Thus, there is transition of $\pi \rightarrow \pi^*$ and $\eta \rightarrow \pi^*$ electrons and in such case the order absorption wavelength is (250-280) nm. The percentage contribution of molecular orbitals along with oscillator strength, energy gap and maximum absorption wavelength is presented in Table 4. The HOMO orbital is 114 and LUMO orbital is 115. The first excited state (HOMO→LUMO (100%)) is calculated as 4.06 eV corresponding to λmax=305.17 nm having minimum oscillator strength=0.0001. This is due to the transition of $\pi \rightarrow \pi^*$ electrons. Similarly, the second excited state is calculated at 275.06 nm (HOMO→L+2 (94%)) with respective excitation energy and oscillator strength 4.51eV and 0.0237. This is due to transition of $\pi \rightarrow \pi^*$ and $eta \rightarrow \pi^*$ electrons.

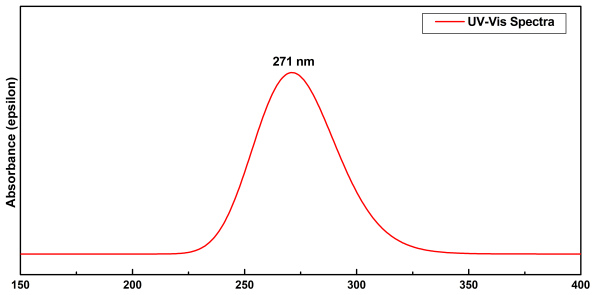

Figure 8: UV-Vis absorbance of GDP in gas phase calculated with TD-B3LYP/6311++G(d,p)

3.7 Molecular Docking

Molecular docking is crucial technique to explore the ligand-protein interaction. The binding sites as well as binding energy, inhibition constant and ligand efficiency are the important parameters which explain the docking analysis of ligand with predicted target (protein) [39, 40]. The target protein Ras-related C3 botulinum toxin substrate 1(RAC1) has been predicted from free online SwissTargetPrediction and two protein 2P2L and 2H7V has been downloaded from protein data bank [41, 42]. The protein has been cleaned by removing the water molecule and co-crystalized ligand. The ligand GDP and proteins 2P2L and 2H7V are prepared for docking by converting them into PDB file. After that the docking has been performed from AutoDock Vina [18]. The binding sites have been examined from Discovery Studio Visualizer 4.5 [19]. Out of the many docked conformers the best docked conformers have been presented in Figure 9. The conventional hydrogen bonds, residue of amino acid, ligand efficiency, inhibition constant and binding energy of ligand-protein interaction is presented in Table 5. From molecular docking analysis it is confirmed that the binding sites in GDP are O2, O3, O5, O7, O10, O31, N29, and H34. During the molecular docking analysis of GDP with Cell division control protein 42 homolog (Cdc42) with the PDB codes 1ANO, 1A4R and 1DOA; the binding sites was found to be almost same [43]. The binding energy for 2P2L (-8.0 kcal/mol) is more than the binding energy of 2H7V (-7.4 kcal/mol). Moreover, the inhibition constant of former (1.35 μM) is less (3.73 μM) than the later one. The number of conventional hydrogen bond in 2P2L is 10 and the number of hydrogen bond in 2H7V is 7. Besides that, the bond length of conventional hydrogen bond in 2P2L is less than that of 2H7V. So, former is better inhibited by title compound.

Table 4: The conventional hydrogen bonds, residue of amino acid, ligand efficiency, inhibition constant, and binding energy of GDP.

Ligand	Protein	PDB code	Bond length (Å)	Binding Atoms	Amino Acid	Binding Energy (kcal/mol)	Inhibition Constant (µM)	Ligand Efficiency
GDP	RAC1	2H7V	2.54	O31	LYS116	–7.4	3.73	0.26
			2.68	O2	LYS16			
			2.28	O7	LYS16			
			2.05	O7	GLY15			
			2.33	O7	VAL14			
			2.00	O7	LYS16			
			2.01	O3	THR17			
GDP	RAC1	2P2L	2.16	N29	SER41	–8.0	1.35	0.29
			2.75	H34	SER41			
			2.80	H34	SER41			
			2.22	O2	LYS16			
			2.45	O2	VAL14			
			2.32	O2	LYS16			
			1.96	O2	GLY15			
			1.75	O3	THR17			
			2.38	O5	LYS16			
			2.31	O10	ALA13			

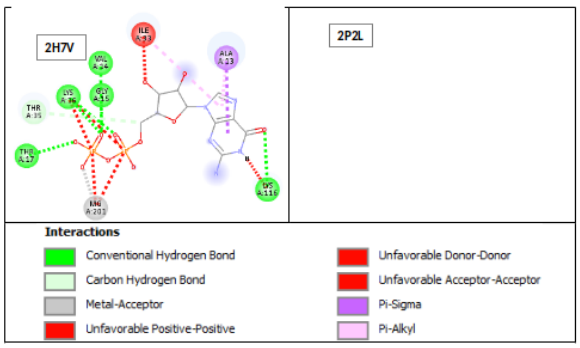

Figure 9: 2-D ligand-protein interaction of GDP with 2H7V and 2P2L PDB code of protein RAC1.

4 Conclusion

The intra-molecular hydrogen bonding of GDP has been scrutinized from QTAIM analysis and RDG scatter plot and its 3D-isosurface. Four intra-molecular hydrogen bonds have been identified and all are partial covalent in nature. Out of them the intra-molecular hydrogen bond H11...O2 is the strongest as it has the smallest bond distance 1.8134 Å and the highest interaction energy (8.3114 kcal/mol). The maximum positive electrostatic potential 113.71 kcal/mol, was observed in H4, and the maximum negative potential associated with O31 of GDP, as predicted by ESP analysis. This analysis confirms that these sites are favourable for intermolecular hydrogen bonding in the solid-state structure of the title compound as well as in ligand-protein interaction analysis. The GDP molecule has 43 atoms and 123 modes of vibrations. All the vibrations are IR and Raman active. The fingerprint and functional group present in the molecule have been explored. There are significant peaks for carbonyl group (C=O), amine group (-NH2), and hydroxyl group (-OH) and phosphate group (PO_4^{2-}). It is confirmed that these functional groups have prominent role for intermolecular hydrogen bonding with residue of amino acid which is verified by the molecular docking as well as Mulliken charge and ESP analysis. UV-Vis spectra analysed that there are single significant absorbance peak at 272 nm wavelength which is correspond to the second excited state (HOMO→L+2 (94%)) with respective excitation energy and oscillator strength 4.51eV and 0.0237. This arises due to transition of $\pi \rightarrow \pi^*$ and $\eta \rightarrow \pi^*$ electrons. Mulliken charge analysis confirmed that the atoms O2, O5, O7, C17, N29, C30, and O31 have negative charge and the atoms P6, N18 and C19 have positive charge. These charges take part in ligand-protein interaction which is explored from molecular docking. The protein 2P2L has more binding affinity than 2H7V protein of RAC1.

Author contribution

M.K. Chaudhary: Conceptualization of research activity, data analysis and manuscript writing; T. Chaudhary: Analysis, and drafting; G.S. Verma: Data calculation; T.R. Paneru: supervision, writing and editing; B.D. Joshi: proofreading and editing and R. K. Shukla: proofreading and editing.

Declarations Conflict of interest

The authors declare no competing interests.

References

[1] L. E. B. Bettio, J. Gil-Mohapel, and A. L. S. Rodrigues. Guanosine and its role in neuropathologies. *Purinergic Signalling*, 12:411–426, 2016.

[2] M. Rathbone, L. Pilutti, F. Caciagli, and S. Jiang. Neurotrophic effects of extracellular guanosine. *Nucleosides, Nucleotides and Nucleic Acids*, 27:666–672, 2008.

[3] L. J. Crane and D. L. Miller. Guanosine triphosphate and guanosine diphosphate as conformation-determining molecules. differential interaction of a fluorescent probe with the guanosine nucleotide complexes of bacterial elongation factor tu. *Biochemistry*, 13(5):933–939, 1974.

[4] F. A. Vaccaro, D. A. Faber, G. A. Andree, D. A. Born, G. Kang, D. R. Fonseca, M. Jost, and C. L. Drennan. Structural insight into g-protein chaperone-mediated maturation of a bacterial adenosylcobalamin-dependent mutase. *J. Biol. Chem.*, 299(9), 2023.

[5] H. Y. Bao, W. Wang, H. B. Sun, and J. Z. Chen. Binding modes of gdp, gtp and gnp to nras deciphered by using gaussian accelerated molecular dynamics simulations. *SAR and QSAR in Environmental Research*, 34(1):65–89, 2023.

[6] G. Rehna, M. I. Ivanov, J. B. Bliska, and C. E. Stebbins. Yersinia virulence depends on mimicry of host rho-family nucleotide dissociation inhibitors. *Cell*, 126(5):869–880, 2006.

[7] M. J. Frisch, G. W. Trucks, H. B. Schlegel, G. E. Scuseria, M. A. Robb, J. R. Cheeseman, G. Scalmani, V. Barone, B. Mennucci, G. A. Petersson, H. Nakatsuji, M. Caricato, X. Li, H. P. Hratchian, A. F. Izmaylov, J. Bloino, G. Zheng, J. L. Sonnenberg, M. Hada, M. Ehara, K. Toyota,

R. Fukuda, J. Hasegawa, M. Ishida, T. Nakajima, Y. Honda, O. Kitao, H. Nakai, T. Vreven, J. A. Montgomery, J. E. Peralta, F. Ogliaro, M. Bearpark, J. J. Heyd, E. Brothers, K. N. Kudin, V. N. Staroverov, R. Kobayashi, J. Normand, K. Raghavachari, A. Rendell, J. C. Burant, S. S. Iyengar, J. Tomasi, M. Cossi, N. Rega, J. M. Millam, M. Klene, J. E. Knox, J. B. Cross, V. Bakken, C. Adamo, J. Jaramillo, R. Gomperts, R. E. Stratmann, O. Yazyev, A. J. Austin, R. Cammi, C. Pomelli, J. W. Ochterski, R. L. Martin, K. Morokuma, V. G. Zakrzewski, G. A. Voth, P. Salvador, J. J. Dannenberg, S. Dapprich, A. D. Daniels, Ö. Farkas, J. B. Foresman, J. V. Ortiz, J. Cioslowski, and D. J. Fox. Gaussian 16 revision, 2016.

[8] C. Lee, W. Yang, and R. G. Parr. Development of the colle-salvetti correlation-energy formula into a functional of the electron density. *Phys. Rev. B*, 37:785–789, 1988.

[9] R. G. Parr and W. Yang. *Density-functional theory of atoms and molecules*. Oxford Univ. Press, New York, NY, 1 edition, 1994.

[10] A. D. Becke. Density-functional thermochemistry. III. the role of exact exchange. *J. Chem. Phys.*, 98:5648–5652, 1993.

[11] T. H. Dunning. Gaussian basis sets for use in correlated molecular calculations. I. the atoms boron through neon and hydrogen. *J. Chem. Phys.*, 90:1007–1023, 1989.

[12] P. Hohenberg and W. Kohn. Inhomogeneous electron gas. *Phys. Rev.*, 136:B864–B871, 1964.

[13] R. Dennington, T. A. Keith, and J. Millam. *GaussView 06*. Shawnee Mission, KS, 2016.

[14] T. A. Keith. Aimall version (19.10.12), 2019.

[15] R. F. W. Bader. *Atoms in molecules: a quantum theory*. Clarendon Press; Oxford University Press, Oxford [England]; New York, 1994.

[16] T. Lu and F. Chen. Multiwfn: A multifunctional wavefunction analyzer. *J. Comput. Chem.*, 33:580–592, 2012.

[17] W. Humphrey, A. Dalke, and K. Schulten. Vmd: Visual molecular dynamics. *J. Mol. Graph.*, 14:33–38, 1996.

[18] O. Trott and A. J. Olson. Autodock vina: Improving the speed and accuracy of docking with a new scoring function, efficient optimization, and multithreading. *J. Comput. Chem.*, 31:455–461, 2010.

[19] *Discovery Studio 4.5 Guide*. San Diego, 2009.

[20] N. M. O'Boyle, A. L. Tenderholt, and K. M. Langner. Cclib: a library for package-independent computational chemistry algorithms. *J. Comput. Chem.*, 29(5):839–845, 2008.

[21] U. Koch and P. L. A. Popelier. Characterization of c-h-o hydrogen bonds on the basis of the charge density. *J. Phys. Chem.*, 99:9747–9754, 1995.

[22] I. Rozas, I. Alkorta, and J. Elguero. Behavior of ylides containing n, o, and c atoms as hydrogen bond acceptors. *J. Am. Chem. Soc.*, 122:11154–11161, 2000.

[23] S. Sarfaraz, M. Yar, M. Ans, M. A. Gilani, R. Ludwig, M. A. Hashmi, M. Hussain, S. Muhammad, and K. Ayub. Computational investigation of a covalent triazine framework (ctf-0) as an efficient electrochemical sensor. *RSC Adv.*, 12:3909–3923, 2022.

[24] E. R. Johnson, S. Keinan, P. Mori-Sánchez, J. Contreras-García, A. J. Cohen, and W. Yang. Revealing non-covalent interactions. *J. Am. Chem. Soc.*, 132:6498–6506, 2010.

[25] T. R. Paneru, M. K. Chaudhary, P. Tandon, and B. D. Joshi. Cocrystal screening of benznidazole based on electronic transition, molecular reactivity, hydrogen bonding, and stability. *J. Mol. Model.*, 30:378, 2024.

[26] G. A. Guirgis, P. Klaboe, S. Shen, D. L. Powell, A. Gruodis, V. Aleksa, C. J. Nielsen, J. Tao, C. Zheng, and J. R. Durig. Spectra and structure of silicon-containing compounds. XXXVI—Raman and infrared spectra, conformational stability, ab initio calculations and vibrational assignment of ethyldibromosilane. *J. Raman Spectrosc.*, 34(4):322–336, 2003.

[27] P. L. Polavarapu. Ab initio vibrational raman and raman optical activity spectra. *J. Phys. Chem.*, 94(21):8106–8112, 1990.

[28] M. P. Andersson and P. Uvdal. New scale factors for harmonic vibrational frequencies using the b3lyp density functional method with the triple-ζ basis set 6-311+g(d,p). *J. Phys. Chem. A*, 109(12):2937–2941, 2005.

[29] R. M. Silverstein, G. C. Bassler, and T. C. Morrill. *Spectrometric identification of organic compounds*. John Wiley and Sons, New York, 4 edition, 1981.

[30] J. Mohan. *Organic Spectroscopy, Principles and Applications*. Narosa Publishing House, New Delhi, 2 edition, 2009.

[31] N. B. Colthup, L. H. Daly, and S. E. Wiberley. *Introduction to Infrared and Raman Spectroscopy*. Academic Press, New York, 1990.

[32] J. S. Murray and P. Politzer. Electrostatic potentials: Chemical applications. In *Encyclopedia of Computational Chemistry*. Wiley, 1 edition, 1998.

[33] T. R. Paneru, M. K. Chaudhary, P. Tandon, T. Chaudhary, and B. D. Joshi. Theoretical study on molecular stability, reactivity, and drug potential of cirsilineol from dft and molecular docking methods. *Chem. Phys. Impact*, 8:100641, 2024.

[34] M. K. Chaudhary, S. Pandey, and P. Tandon. Frontier molecular orbitals, mep, nbo, and vibrational spectra of mesalamine: A first principle study from dft and molecular docking approaches. *Scientific World*, 17(17):27–36, 2024.

[35] A. Mandru, J. Mane, and R. Mandapati. A review on uv-visible spectroscopy. *Journal of Pharma Insights and Research*, 1(2):91–96, 2023.

[36] A. Ciesielska, J. Brzeski, D. Zarzeczańska, M. Stasiuk, M. Makowski, and S. Brzeska. Exploring the interaction of biologically active compounds with dna through the application of the switchsense technique, uv–vis spectroscopy, and computational methods. *Spectrochimica Acta Part A: Molecular and Biomolecular Spectroscopy*, 316:124313, 2024.

[37] C. S. Abraham, S. Muthu, J. C. Prasana, S. Armaković, S. J. Armaković, and B. Geoffrey. Computational evaluation of the reactivity and pharmaceutical potential of an organic amine: A dft, molecular dynamics simulations and molecular docking approach. *Spectrochim. Acta A Mol. Biomol. Spectrosc.*, 222:117188, 2019.

[38] A. Singhal, U. Saini, B. Chopra, A. K. Dhingra, A. Jain, and J. Chaudhary. Uv–visible spectroscopy: A review on its pharmaceutical and bio-allied sciences applications. *Curr. Pharm. Anal.*, 20(3):161–177, 2024.

[39] M. K. Chaudhary, P. Prajapati, K. Srivastava, K. F. Silva, B. D. Joshi, P. Tandon, and A. P. Ayala. Molecular interactions and vibrational properties of ricobendazole: Insights from quantum chemical calculation and spectroscopic methods. *J. Mol. Struct.*, 1230:129889, 2021.

[40] M. K. Chaudhary, A. Srivastava, K. K. Singh, P. Tandon, and B. D. Joshi. Computational evaluation on molecular stability, reactivity, and drug potential of frovatriptan from dft and molecular docking approach. *Comput. Theor. Chem.*, 1191:113031, 2020.

[41] A. Daina, O. Michielin, and V. Zoete. Swisstargetprediction: updated data and new features for efficient prediction of protein targets of small molecules. *Nucleic Acids Res.*, 47(W1):W357–W364, 2019.

[42] P. W. Rose, B. Beran, C. Bi, W. F. Bluhm, D. Dimitropoulos, D. S. Goodsell, A. Prlić, M. Quesada, G. B. Quinn, J. D. Westbrook, J. Young, B. Yukich, C. Zardecki, H. M. Berman, and P. E. Bourne. The rcsb protein data bank: redesigned web site and web services. *Nucleic Acids Res.*, 39:D392–D401, 2011.

[43] M. K. Chaudhary, B. Maharjan, G. S. Verma, and R. K. Shukla. Hydrogen bonding and reactivity behavior of guanosine-5'-diphosphate from dft and molecular docking approach. *Api J. Sci.*, 1:84–91, 2024.